CMOS-Compatible Plasmonic Bragg Reflectors Based on Cu-Dielectric-Si Structures

Shiyang Zhu, Hong-Son Chu, G. Q. Lo, and D. L. Kwong

***Abstract*—Cu-dielectric-Si hybrid plasmonic waveguide (HPW) based plasmonic Bragg reflectors (PBRs) are fabricated on SOI platform using standard CMOS technology and characterized in the 1515–1615-nm wavelength range. Optical stop-bands are experimentally observed, depending on the grating size and the number of grating periods. PBRs with 20 periods exhibit ~-30-dB transmission within the stop-band, ~-10-dB transmission outside the stop-band (both are normalized by the corresponding 2-μm-long straight HPW), steep band edges of ~0.92dB/nm, and small ripples in the transmission spectra beyond the band edges, in agreement with those predicted from FDTD simulations. These favorable performances, together with ease fabrication and CMOS compatibility, make the proposed HPW-based PBRs useful for dense Si photonic integrated circuits.**

***Index Terms*— Bragg grating, hybrid plasmonic waveguide, integrated photonics, CMOS compatibility.**

I. Introduction

Owing to the ability of tight light confinement beyond the diffraction limit, plasmonics provides a potential way to miniaturize footprints of photonic devices and increase densities of electronic and photonic integrated circuits (EPICs) [1]. As an essential component of many photonic devices, plasmonic Bragg reflectors (PBRs) have been widely investigated [2-6], mostly based on metal-insulator-metal (MIM) waveguides [2-5] which provide tight mode confinement but suffer from large propagation loss. MIM-based PBRs usually require non-CMOS-compatible technology for fabrication [5], thus making it difficult to implement in Si EPICs. In contrast, hybrid plasmonic waveguides (HPWs), which consist of a low-index dielectric gap sandwiched between a metal and a high-index core, provide a better tradeoff between the mode confinement and propagation loss [7,8]. Indeed, several kinds of HPW-based PBRs have been proposed theoretically, either with periodic variations of the thickness of the low-index layer [9], the height of the high-index Si core [10], or the width of the Si core and the SiO_2 slots [11] in HPWs, or with periodic rectangular air holes inside the Si core of a Si-air-Ag HPW [12]. However, experimental realizations of HPW-based PBRs have not been reported yet.

Recently a CMOS-compatible HPW with vertical Cu-SiO_2-Si structure has been developed and various passive components including bends, power splitters, and ring resonators have been realized on a SOI platform [13,14]. Cu is chosen as the metal because of CMOS compatibility and relatively low metal loss around 1.55-μm telecom wavelengths [15]. Moreover, attractive properties may be introduced if the SiO_2 layer between the Cu-cap and Si core is replaced by a functional dielectric, e.g. TiO_2 [16,17]. The potential of this Cu-dielectric-Si HPW can be further exploited to design and realize more sophisticated and/or new functional plasmonic components. In this letter, we present numerical and experimental demonstration of PBRs based on this HPW.

II. Design and Simulation

Fig. 1 shows the schematic diagram of HPW proposed in this work. The Cu-capped area, which is defined as the plasmonic area, is connected with the input/output Si channel waveguides through 2-μm-long taper couplers. The PBR is formed by periodically interrupting the Si core of the straight HPW along the propagation direction x to form N identical Si pillars with length of d_1 and interval (between two Si pillars) of d_2. The Si cores of HPW and the Si pillars have the same width (W_P) and height (h_{Si}), thus they can be fabricated in the same process without additional steps. The grooves between Si pillars are filled by plasma-enhanced chemical vapor deposited (PECVD) SiO_2, followed by chemical mechanical polishing (CMP), as shown in Fig. 1(b). It actually contains two periodically concatenated waveguide subsections along the x-direction: one is Cu-dielectric-Si and the other is Cu-dielectric-SiO_2.

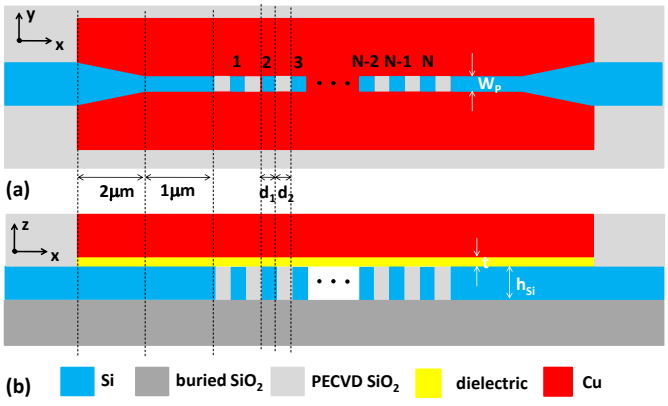

Fig. 1. Schematic diagram of the Cu-dielectric-Si HPW based PBR inserted in the Si channel waveguide (a) top view and (b) cross sectional view.

Manuscript received August 4, 2013; revised August 27, 2013; accepted September 12, 2013. This work was supported by Singapore SERC/A*STAR Grant 092-154-0098.

S. Y. Zhu, G. Q. Lo, and D. L. Kwong are with the Institute of Microelectronics, A*STAR (Agency for Science, Technology and Research), Singapore 117685, Singapore (phone: 65-67705746; fax: 65-67731914; e-mail: zhusy@ime.a-star.edu.sg). H. S. Chu is with Advanced Photonics and Plasmonics Group, Institute of High Performance Computing, A*STAR, Singapore 138632, Singapore.

Color versions of one or more of the figures in this letter are available online at http://ieeexplore.ieee.org

Digital Object Identifier xxxxxxx.

Fig. 2 shows electric field (|E|) distribution of the fundamental 1550-nm transverse magnetic (TM) mode in these two waveguide subsections, calculated using the eigen-mode expansion (EME) method [18]. The structural parameters are set as W_P = 300 nm, h_{Si} = 220 nm, and dielectric thickness = 32 nm. The complex indices of SiO_2, Si, dielectric (here, TiO_2 [19]), and Cu [20] at 1550 nm are set as 1.445, 3.455, 2.2, and 0.282+11.8i, respectively. The mode is tightly confined in the thin dielectric layer of the Cu-dielectric-Si subsection and is loosely confined in the bottom SiO_2 layer of the Cu-dielectrc-SiO_2 subsection. The effective mode indices (n_{eff}) are 2.52+0.0072i for the former and 0.82+0.0030i for the latter. n_{eff} can be modified by varying the structural parameters.

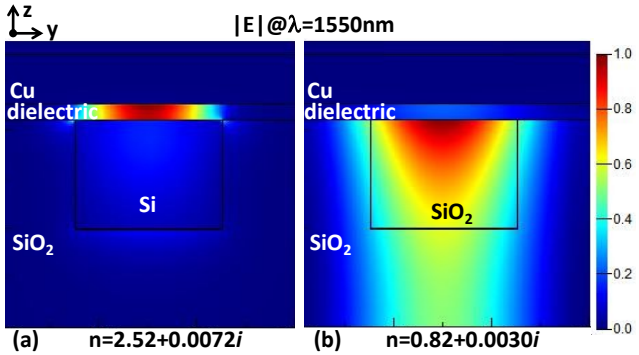

Fig. 2. Electric field (|E|) distributions of the fundamental 1550-nm TE mode in (a) Cu-dielectric-Si and (b) Cu-dielectric-SiO_2, calculated using the EME method.

The Bragg wavelength (i.e., the central wavelength of the stop-band, λ_b) can be formulated by the grating equation as:

$$d_1 \,\mathrm{Re}(n_{eff,1}) + d_2 \,\mathrm{Re}(n_{eff,2}) = \lambda_b / 2 \qquad (1)$$

and the width of the stop-band is approximated as:

$$\Delta\omega_g = \omega_c \frac{4}{\pi} \sin^{-1} \frac{\mathrm{Re}(n_{eff,1}) - \mathrm{Re}(n_{eff,2})}{\mathrm{Re}(n_{eff,1}) + \mathrm{Re}(n_{eff,2})} \qquad (2)$$

where ω_c is the central frequency of the stop-band.

The transmission spectra of PBRs are calculated using three-dimensional finite-difference-time-domain (3D-FDTD) simulations [18]. For simplicity, we set $d_1 = d_2 = d$, 1-μm long straight HPW before and after the PBR, and other parameters as the abovementioned. The source is set to have a 1.3–1.8-μm spectral range and is located at 1 μm before the PBR. Fig. 3(a) plots transmission spectra for PBRs with d = 220 nm and periods (i.e., the number of Si pillars, N) of 5, 10, 15, or 20, normalized by that of the corresponding 2-μm-long straight HPW. A stop-band is clearly observed at λ_b ~1520 nm, which is slightly larger than that calculated from Eq. 1 (~1470 nm) using the EME calculated n_{eff} values. The transmission level within the stop-band is reduced with increasing N, reaching minimum of ~-40 dB at N = 15. Further increasing N will not reduce the transmission level but make the band edge steeper. Therefore, we set N = 15 in the following simulations. The transmission level in the right pass-band (the longer wavelength side) depends on N weakly while that in the left pass-band (the shorter wavelength side) decreases with increasing N, which may be attributed to the larger metal loss of Cu at the shorter wavelength [20]. Fig. 3(b) plots the normalized transmission spectra for PBRs with 15 periods and different d values of 200–240 nm. They exhibit similar profiles and the stop-band shifts to longer wavelength with d increasing, qualitatively agrees with that predicted from Eqs. (1) and (2). However, the values of $\Delta\omega_g$ and λ_b-shift read from Fig. 3(b) are smaller than those calculated from Eqs. (1) and (2). This quantitative disagreement, together with the larger λ_b compared with that calculated from Eq. (1), indicates that the effective indices of two waveguide subsections may differ from those calculated from the EME method, probably because the optical field distributions in the Cu-TiO_2-Si and Cu-TiO_2-SiO_2 subsections may influence each other, as observed in Fig. 4(b). The apparent double minima within the stop-band in Fig. 4(b) may originate from excitation of high-order modes or simply from the possible calculation error.

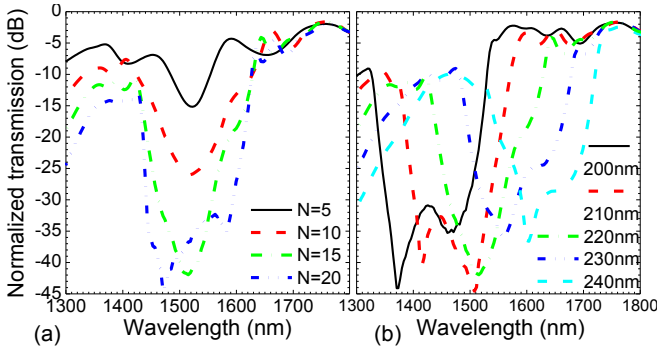

Fig. 3. FDTD calculated transmission spectra for (a) PBRs with d = 220 nm and different periods and (b) PBRs with 15 periods and different d values, normalized by that of the corresponding 2-μm-long HPW.

Fig. 4 shows snapshots of the propagating mode's field patterns obtained from the FDTD simulation. The d = 220 nm PBR is within the stop-band at λ = 1556 nm, one sees in Fig. 4(a) that the light is strongly reflected to the input HPW, causing an oscillating field distribution map in the input HPW. The PBR is outside the stop-band at λ = 1645 nm, one sees in Fig. 4(b) that the light transmits through the PBR to the output HPW with an insertion loss of ~3.5 dB. At λ = 1645 nm, the d = 220 nm PBR is still within the stop-band, one sees in Fig. 4(c) that the light is strongly reflected.

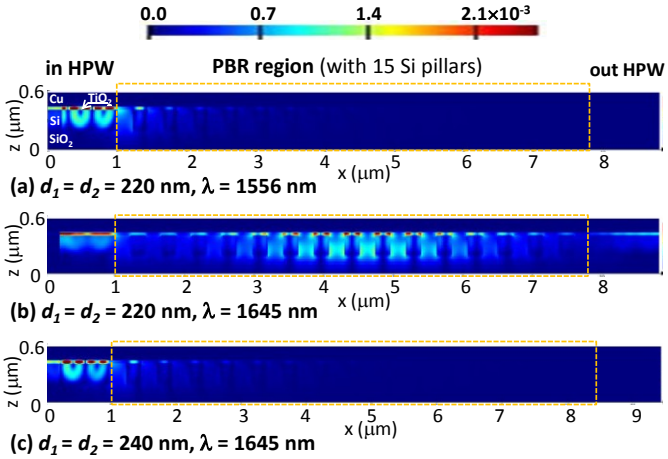

Fig. 4. Distribution of the absolute value of Poynting vector along the PBR with 15 periods includes 1-μm-long input/output HPWs: (a) $d_1 = d_2$ = 220 nm, λ = 1556 nm, (b) $d_1 = d_2$ = 220 nm, λ = 1645 nm, and (c) $d_1 = d_2$ = 240 nm, λ = 1645 nm.

The real devices may deviate from the above ideal design due to the imperfect fabrication. When d_1 has a deviation Δd,

d_2 has an according deviation -Δd, as shown in the top of Fig. 5(a). Normalized transmission spectra for PBRs with Δd of -20–+20 nm are plotted in Fig. 5(a). They exhibit almost similar profiles while λ_b shifts to shorter wavelength with Δd increasing, as predicted from Eq. (1). It indicates that the proposed PBRs have a large Δd tolerance. Fig. 5(b) plots normalized transmission spectra for PBRs whose Si pillars have an angled sidewall along the x-direction and the bottom length of the Si pillars keeps 220 nm. With θ increasing, the stop-band shows blue-shift because the effective d_1 (d_2) decreases (increases), and the transmission within the stop-band increases because the reflection at the angled Si/SiO_2 interfaces becomes weaker. Nevertheless, the PBR's performance keeps almost unchanged when θ is larger than 80°, indicating that the proposed PBRs also have a large θ tolerance.

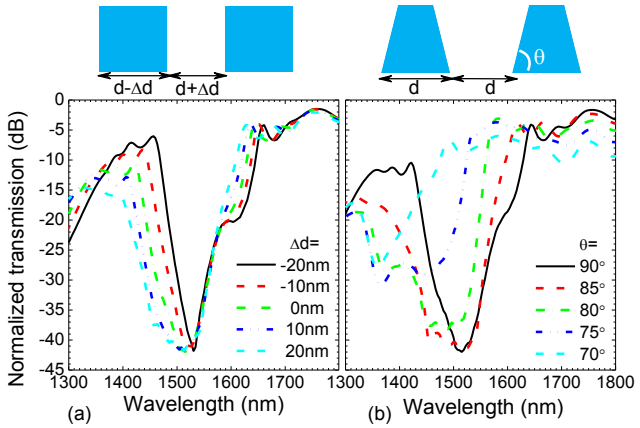

Fig. 5. FDTD calculated transmission spectra for PBRs with 15 periods, normalized by that of the corresponding 2-μm-long HPW: (a) Si pillars have a length deviation Δd, i.e., d_1 = 220 nm - Δd and d_2 = 220 nm + Δd, as shown in the left inset, and (b) the Si pillars (the length at the bottom keeps $d_1 = d_2 = d$ = 200 nm) have a sidewall angle θ, as shown in the right inset.

III. Experimental Demonstration

The PBRs were fabricated on SOI wafers with 220-nm top Si and 2-μm buried oxide using standard CMOS technology. The fabrication processes are essentially the same as those for the other HPW-based passive devices reported elsewhere [16]. In the mask layout, the grating size is set as $d_1 = d_2$ = 0.2, 0.21, 0.22, 0.23, or 0.24 μm and the number of periods is set as N = 10, 15, or 20. Other parameters are set as those indicated in Fig. 1. The critical dimension of Si pillars was further tuned by varying the exposure dose during UV lithography. Fig. 6(a) is a microscopic picture of one of the fabricated devices. The Cu-capped plasmonic area is inserted in the conventional Si channel waveguide. Fig. 6(b) is a cross sectional transmission electron microscopy (XTEM) image along the x-z plane for a PBR having 10 Si pillars. Fig. 6(c) is the zoom-in image of Fig. 6(b), showing part of the input HPW and the first 2 Si pillars. Fig. 6(d) is a XTEM image along the y-z plane. The dielectric between the Cu-cap and the Si core is a 32-nm-thick sputtering-deposited TiO_2 layer. The diced chips were measured using the conventional fiber-waveguide-fiber method. The input light is quasi-TM light from a broadband (~1515–1615 nm) laser source and the output light is measured by a power meter and an optical spectrum analyzer (OSA).

Straight HPWs with different lengths and a reference Si channel waveguide without the plasmonic area on the same chip were measured. Using the cut-back method the propagation loss is extracted to 0.22±0.01 dB/μm and the coupling loss between the Si channel waveguide and the HPW through the 2-μm-long taper coupler is 1.8±0.1 dB/facet, close to the theoretical prediction, and also in agreement with the previous report [16].

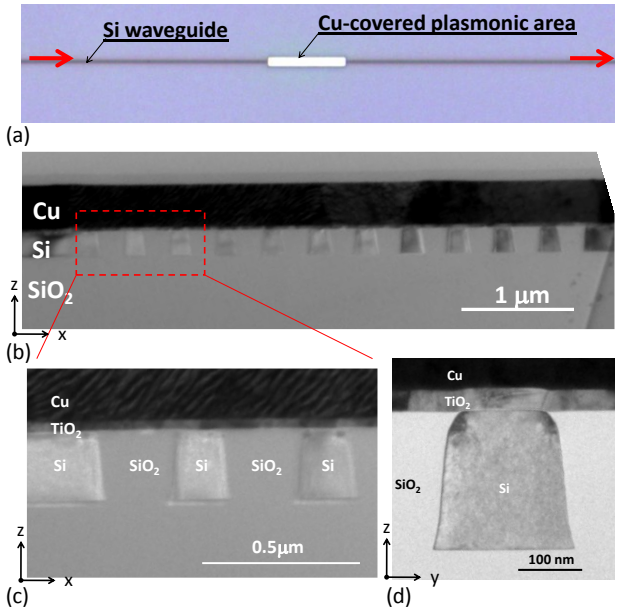

Fig. 6. (a) Microscopic photograph of one of the fabricated PBRs, (b) XTEM image in the x-z plane of a PBR having 10 Si pillars, (c) zoom-in image of (b), and (d) XTEM image in the y-z plane.

Fig. 7 plots spectra measured on a set of PBRs with d = 230 nm and different periods N = 10, 15, and 20, respectively, normalized by that measured on the corresponding 2-μm-long straight HPW. Since the spectral range of our broad-band laser source (~100 nm) is smaller than the width of stop-band assessed from Fig. 3 (~174 nm), only the right side of the stop-band is observed. The transmission level inside the stop-band decreases with N increasing and that outside the stop-band (i.e., the insertion loss) depends on N weakly, in agreement with that observed in Fig. 3(a). However, compared with Fig. 3(a), more periods are required for the minimum transmission in the stop-band and the insertion loss is larger, which may be simply attributed to the imperfect fabrication such as the non-ideal Si core cross section as shown in Fig. 6 and the surface/sidewall roughness of Si, TiO_2, and Cu. Nevertheless, the fabricated PBR with 20 periods (total length of ~10 μm) already exhibits favorable performance such as low transmission of ~-30 dB within the stop-band, insertion loss of ~-10 dB outside the stop-band, steep band edges of ~0.92 dB/nm, and small ripples in the transmission spectra beyond the band edges. The steepness of the experimental stop-band edge is close to that read from Fig. 3(a) for the N = 20 PBR (~0.9 dB/nm). It indicates that the steepness is mainly determined by N, rather than the Si pillar cross section, at least when θ is larger than ~80°, as observed in Fig. 5(b). The other performances (i.e., the insertion loss and the transmission within the stop-band) may be further improved by improving

the fabrication.

Fig. 8 plots normalized spectra measured on other set of PBRs which have 20 periods and 5 different d values ranging from 200 to 240 nm. They show a clear stop-band shift, as that observed in Fig. 3(b). For PBRs with d of 200 and 210 nm, the detection range (1510–1610 nm) is outside their stop-band. The measured spectra are in the right pass-band, which exhibit small ripples and weak wavelength dependence. The stop-band shifts to longer wavelength with d increasing. We see that the right band edges for PBRs with d of 220 nm and 230 nm move in the detection range. The band edge is observed around 1520 nm for the BPR with d of 220 nm and around 1566 nm for that with d of 230 nm. The $\Delta\lambda_b/\Delta d$ value is calculated to be ~46, quantitatively agrees with that calculated from Fig. 3(b). For the PBR with d of 240 nm, the detection range is within its stop-band, the measured spectrum exhibits small transmission level of ~-30 dB. One can expect that the left band edge will move in the detection range when d further increasing.

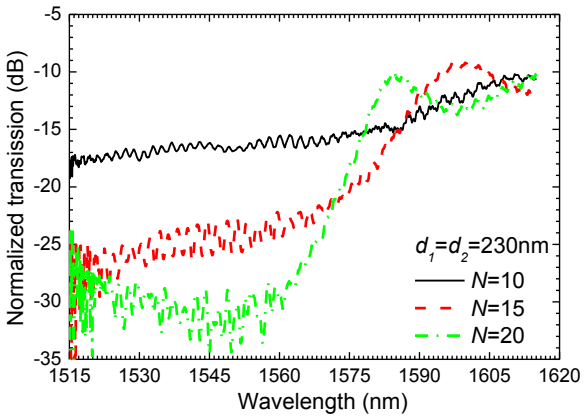

Fig. 7. Transmission spectra measured on PBRs with d = 230 nm and different periods of 10, 15, or 20, normalized by that measured on the corresponding 2-μm-long straight HPW.

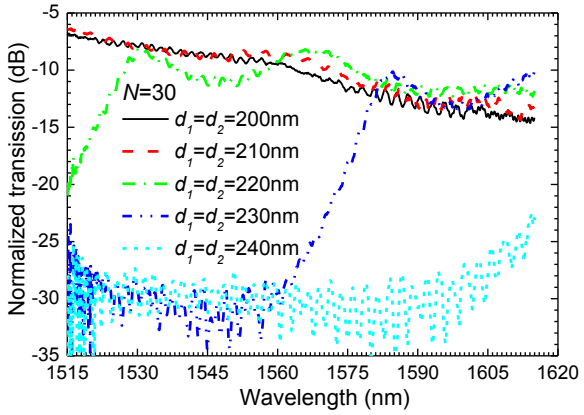

Fig. 8. Transmission spectra measured on PBRs with 20 periods and different d of 200, 210, 220, 230, and 240 nm, normalized by that measured on the corresponding 2-μm-long straight HPW.

IV. Conclusion

In summary, a novel HPW-based PBR is proposed. FDTD numerical simulation shows it has favorable performance such as high reflection within the stop-band, high transmission outside the stop-band, steep band edge, and small ripples in the pass-band spectra, as well as large fabrication tolerance. The proposed PBRs are realized on a SOI platform using standard CMOS technology and measured in the 1515–1615-nm wavelength range. The measurement results agree well with those predicted from FDTD simulations. This favorable result, combined with full CMOS compatibility and ease fabrication, indicates that the proposed PBR is an attractive component to be seamlessly integrated in dense Si EPICs.

References

[1] D. K. Gramotnev and S. I. Bozhevolnyi, "Plasmonics beyond the diffraction limit," *Nat. Photon*., vol. 4, no. 2, pp. 83-91, Feb. 2010.

[2] J. Q. Liu, L. L. Wang, M. D. He, W. Q. Huang, D. Wang, B. S. Zou, and S. Wen, "A wide bandgap plasmonic Bragg reflector," *Opt. Express*, vol. 17, no.7, pp. 4888-4894, Mar. 2008.

[3] A. Hosseini, H. Nejati, and Y. Massoud, "Modeling and design methodology for metal-insulator-metal plasmonic Bragg reflectors," *Opt. Express*, vol. 16, no. 3, pp. 1475-1480, Feb. 2008.

[4] Y. Liu, Y. Liu, and J. Kim, "Characteristics of plasmonic Bragg reflectors with insulator width modulated in sawtooth profiles," *Opt. Express*, vol. 18, no. 11, pp. 11589-11598, May 2010.

[5] P. Neutens, L. Lagae, G. Borghs, and P. Van Dorpe, "Plasmon filters and resonators in metal-insulator-metal waveguides," *Opt. Express*, vol. 20, no. 4, pp. 3408-3423, Feb. 2012.

[6] V. S. Volkov, S. I. Bozhevolnyi, E. Devaux, J. Y. Laluet, and T. W. Ebbesent, "Wavelength selective nanophotonic components utilizing channel plasmon polaritons," *Nano Lett.*, vol. **7**, no. 4, pp. 880-884, Apr. 2007.

[7] R. F. Oulton, V. J. Sorger, D. A. Genov, D. F. P. Pile, and X. Zhang, "A hybrid plasmonic waveguide for subwavelength confinement and long-range propagation," *Nat. Photon*., vol. 2, no. 8, pp. 496-500, Aug. 2008.

[8] H. S. Chu, E. P. Li, P. Bai, and R. Hegde, "Optical performance of single-mode hybrid dielectric-loaded plasmonic waveguide-based components," *Appl. Phys. Lett*., vol. 96, no. 22, art. 221103, Jun. 2010.

[9] P. Xu, Q. Huang, and Y. Shi, "Silicon hybrid plasmonic Bragg grating reflectors and high Q-factor micro-cavities," *Opt. Commun.*, vol. 289, pp. 81-84, Feb. 2013.

[10] J. Xiao, J. Liu, Z. Zheng, Y. Bian, G. Wang, and S. Li, "Transmission performance of a low-loss metal-insulator-semiconductor plasmonic phase-shift Bragg grating," *Phys. Status Solidi A,* vol. 209, no. 8, pp. 1552-1556, Jun. 2012.

[11] L. Lu, F. Li, M. Xu, T. Wang, J. Wu, L. Zhou, and Y. Su, "Mode-selective hybrid plasmonic Bragg grating reflector," *IEEE Photon. Techn. Lett.,* vol. 24, no. 19, pp. 1765-1767, Oct. 2012.

[12] X. Yang, A. Ishikawa, X. Yin, and X. Zhang, "Hybrid photonic-plasmonic crystal nanocavities," *ACS Nano*, vol. 5, no. 4, pp. 2831-2838, Mar. 2011.

[13] S. Y. Zhu, G. Q. Lo, and D. L. Kwong, "Experimental demonstration of vertical Cu-SiO_2-Si hybrid plasmonic waveguide components on an SOI platform," *IEEE Photon. Techn. Lett.*, vol. 24, no. 14, pp. 1224-1226, Jul. 2012.

[14] S. Y. Zhu, G. Q. Lo, and D. L. Kwong, "Performance of ultracompact copper-capped silicon hybrid plasmonic waveguide-ring resonators at telecom wavelengths," *Opt. Express*, vol. 20, no. 14, pp. 15232-15246, Jul. 2012.

[15] H. S. Lee, C. Awada, S. Boutami, F. Charra, L. Douillard, and R. E. de Lamaestre, "Loss mechanisms of surface plasmon polaritons propagation on a smooth polycrystalline Cu surface," *Opt. Express*, vol. 20, no. 8, pp. 8974-8981, Apr. 2012.

[16] S. Y. Zhu, G. Q. Lo, J. L. Xie, and D. L. Kwong, "Toward athermal plasmonic ring resonators based on Cu-TiO_2-Si hybrid plasmonic waveguide", *IEEE Photon. Techn. Lett*., vol. 25, no. 12, pp. 1161-1164, Jun. 2013.

[17] S. Y. Zhu, G. Q. Lo, and D. L. Kwong, "Theoretical investigation of ultracompact and athermal Si electro-optic modulator based on Cu-TiO_2-Si hybrid plasmonic donut resonator," *Opt. Express*, vol. 21, no. 10, pp. 12699-12712, May 2013.

[18] (2013) Lumerical Solutions [Online]. Available: http://www.lumerical.com.

[19] G. Gulsen and M. N. Inci, "Thermal optical properties of TiO_2 films," *Opt. Mater*., vol. 18, no. 4, pp. 373-381, Jan. 2002.

[20] S. Roberts, "Optical properties of copper," *Phys. Rev.*, vol. 118, no. 6, pp. 1509-1518, Jun. 1960.